ARTICLES
https://doi.org/10.1038/s41557-022-00928-x

nature chemistry

Check for updates

Tunable acetylene sorption by flexible catenated metal–organic frameworks

Mickaele Bonneau[1], Christophe Lavenn[2], Jia-Jia Zheng[1,3], Alexandre Legrand[1], Tomofumi Ogawa[2], Kunihisa Sugimoto[1,4], Francois-Xavier Coudert[5], Regis Reau[6], Shigeyoshi Sakaki[3], Ken-ichi Otake[1] and Susumu Kitagawa[1]✉

The safe storage of flammable gases, such as acetylene, is essential for current industrial purposes. However, the narrow pressure (*P*) and temperature range required for the industrial use of pure acetylene (100 < *P* < 200 kPa at 298 K) and its explosive behaviour at higher pressures make its storage and release challenging. Flexible metal–organic frameworks that exhibit a gated adsorption/desorption behaviour—in which guest uptake and release occur above threshold pressures, usually accompanied by framework deformations—have shown promise as storage adsorbents. Herein, the pressures for gas uptake and release of a series of zinc-based mixed-ligand catenated metal–organic frameworks were controlled by decorating its ligands with two different functional groups and changing their ratio. This affects the deformation energy of the framework, which in turn controls the gated behaviour. The materials offer good performances for acetylene storage with a usable capacity of ~90 v/v (77% of the overall amount) at 298 K and under a practical pressure range (100–150 kPa).

The development of new technologies for efficient gas storage at ambient pressure can improve safety and provide new possibilities for gas cylinder design. The usable gas capacity, which differs from the maximum quantity adsorbed, under mild pressure and temperature conditions is another concern for researchers. In contrast to gases such as carbon dioxide, methane, oxygen and nitrogen, which have wider compression pressure tolerances, pure acetylene gas is challenging to handle and safely store due to its explosive behaviour when compressed over 200 kPa at room temperature. Consequently, in the last century, cylinders have been filled with acetylene dissolved at high pressure ($P > 1{,}500$ kPa) in a solvent such as acetone[1–3]. However, such an acetylene commercial set-up could contaminate the acetylene gas. When cylinders are filled with pure acetylene gas at 200 kPa (safe pressure), it allows the release of only 50% of its total capacity at 100 kPa (the limit pressure for the gas to flow spontaneously), keeping 50% unused, which is not economically useful, and is potentially dangerous. The creation of porous materials capable of delivering large quantities of pure acetylene in a highly narrow pressure range (100–150 kPa) at room temperature is therefore essential[4].

As a potential solution, porous materials, particularly metal–organic frameworks (MOFs) or porous coordination polymers, possess inherent voids that allow the storage and delivery of large amounts of gases[5–8]. In contrast to rigid materials showing a Langmuir type I isotherm, flexible MOFs, also called soft porous crystals, possess both ordered network and structural transformability, resulting in a sigmoidal S-shape isotherm and higher usable storage capacity when the gate pressures are in the desired working pressure range (Fig. 1)[9–12].

The flexibility depends not only on the binding capacity and mobility of unit ligands and metal ions but also on other factors, including the deformation of the entire framework as a result of the guest molecules in the pores[13–15]. Strategies using ligand functionalization have been developed to investigate the behaviour and properties of flexible MOFs[16–21]. Still, none of them focused on gas storage and especially sensitive gas, which mandates strict temperature and pressure conditions[22–27].

Regarding acetylene storage, rigid and flexible MOFs have demonstrated high adsorption capacities at 298 K and 100 kPa. However, the desorption pressure does not match the acetylene storage requirements for safe handling described above. All the MOFs reported for their high acetylene capacities were recorded at a pressure of 100 kPa, which is below the ideal working pressure range[28–32]. Speculative values were also calculated for acetylene adsorption at high pressure ($P > 3{,}500$ kPa), far above the explosion limit for acetylene[32]. Herein, we demonstrate the optimum pressure range for stable acetylene storage while maintaining high deliverable capacity[33–36]. To the best of our knowledge, acetylene sorption isotherms on MOFs at a pressure range between 100–150 kPa have not been reported so far.

We used a doubly catenated structure—that is, doubly interpenetrated, or twofold interlocked—as a soft porous crystal candidate: $[Zn_2(bdc)_2(4,4'\text{-bpy})]$ where bdc = 1,4-benzenedicarboxylic acid and 4,4′-bpy = 4,4′-bipyridine (**Zn-CAT**), where the mutual dislocation of the two identical framework motifs can introduce acetylene, displaying a sigmoidal sorption isotherm. The gate-opening and gate-closing pressures (P_{go} and P_{gc}) depend on the deformation energy to create space, attributed to the interaction between the two interpenetrating frameworks[37,38]. Therefore, the isotherm can be controlled by the steric and electronic properties of the organic linker (L) of the framework. At a certain temperature, T, the isotherm is a function (F) of P and L as $A_T = F(P, \text{L})$ (A_T denotes the adsorption amount at T; Fig. 1). The introduction of different ratios of functionalized bdc–X linkers (X = $-NO_2$ or $-NH_2$) allows the

[1]Institute for Integrated Cell-Material Sciences (WPI-iCeMS), Kyoto University, Sakyo-ku, Japan. [2]Air Liquide Laboratories, Innovation Campus Tokyo, Yokosuka, Japan. [3]Element Strategy Initiative for Catalyst and Batteries, Kyoto University, Nishikyo-ku, Japan. [4]Japan Synchrotron Radiation Research Institute/SPring-8, Sayo, Japan. [5]Chimie Paris Tech, PSL University, CNRS, Institut de Recherche de Chimie Paris, Paris, France. [6]Air Liquide R&D, Les Loges-en-Josas, France. ✉e-mail: kitagawa@icems.kyoto-u.ac.jp

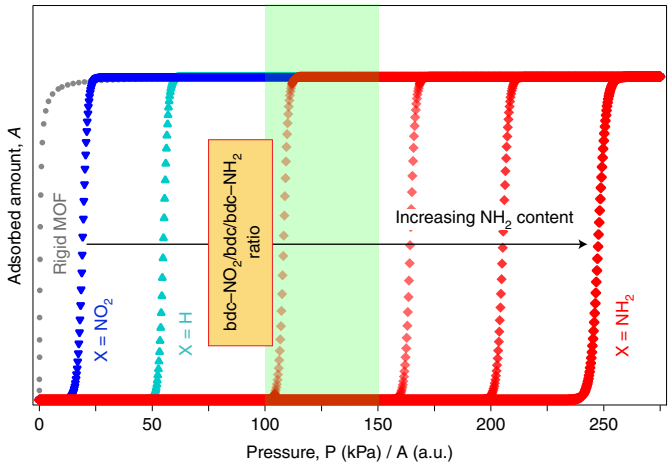

Fig. 1 | Schematic representation of the S-shape adsorption isotherms of Zn-CAT-(X)*n* depending on guest pressure and the ratio of bdc-NO_2/bdc/bdc-NH_2 linkers in the MOF. A type I adsorption isotherm of a rigid MOF is shown in grey for comparison. The functionalization of **Zn-CAT** (light blue triangles) leads to a shift in the gate pressure to the lower pressure with increasing NO_2 functionalization (dark blue inverse triangles) or higher pressure range with increasing NH_2 functionalization (various shades of red diamonds). The green area represents the targeted practical range (100–150 kPa) for safe acetylene use.

optimization of the sigmoidal sorption at arbitrary temperature storage (typically room temperature) and 100 kPa release of acetylene. The strategy of deformation energy control, as devised for acetylene, is also applicable to CO_2, O_2 and CH_4 gases, in which lower filling and release pressures are preferable for the safer use of the gas cylinder.

Results and discussion

Synthesis and characterization. A series of **Zn-CAT** derivatives composed of a mixture of bdc and a substituted bdc–X (X = $-NO_2$ or $-NH_2$) ligands was synthesized with precise control of the bdc/bdc–X ratio (Fig. 2a–c and Supplementary Fig. 1)[37]. The final linker ratio of these $[Zn_2(bdc)_{2-a}(bdc–X)_a(bpy)]$ materials (with a varying from 0 to 2) was confirmed by ^{1}H NMR and showed almost no deviation from the linker ratio expected from the introduced mixture (Fig. 2c and Supplementary Figs. 2–14). The samples were designated according to Zn-CAT-$(X)_n$, that is, showing the functional moiety (X = $-NH_2$, $-NO_2$) and molar percent (n = 0–100%) for clarity. All materials were thermally stable up to 623 K, as observed by thermogravimetric analysis (Supplementary Figs. 15–17). The scanning electron microscopy images of the as-synthesized samples were then analysed and exhibited homogeneity of particle sizes in the micrometre range (Supplementary Figs. 18 and 19). Powder X-ray diffraction patterns, infrared analysis, ultraviolet–visible absorption spectroscopy and crystal structures of the as-synthesized and activated samples confirmed the purity of all materials as well as their isostructural nature (Supplementary Figs. 20–26 and Supplementary Tables 1 and 2). Interpenetrated **Zn-CAT** shows a dynamic transition from the closed form (when the structure is completely evacuated from guests) to the open form (when a specific gas pressure or temperature is applied)[39]. Thus, the gas sorption properties of the **Zn-CAT-$(X)_n$** series were investigated.

First, **Zn-CAT-$(X)_n$** samples were confirmed to behave as a solid solution; that is, the ligands were homogeneously distributed within the backbone structures (Supplementary Fig. 27)[40,41]. The influence of the ratio of linker mixture on the P_{go} and P_{gc} pressures was determined from single gas adsorption measurements performed at different temperatures and pressures (Fig. 3 and Supplementary Figs. 28–36). Acetylene physisorption of pristine **Zn-CAT** at 273 K showed P_{go} = 44 kPa and P_{gc} = 19 kPa with an excess amount of 2.87 mol mol^{-1} of acetylene adsorbed (Fig. 3)[39]. When **Zn-CAT-$(NH_2)_n$** is used, a shift in P_{go} from 48 to 83 kPa was observed as n increased from 5 to 60% (Fig. 3a). By contrast, for **Zn-CAT-$(NO_2)_n$**, the gate-opening pressure shifted to a lower pressure when n increased from 5 to 100% (from P_{go} = 31 kPa to P_{go} = 1 kPa; Fig. 3b). The plot of the gate-opening and gate-closing pressures as a function of the molar percentage of amino groups in **Zn-CAT-$(NH_2)_n$** suggests that P_{go} increases exponentially with the amount of bdc–NH_2 incorporated (Fig. 3c). At a higher molar percentage (n > 60%) of bdc–NH_2, P_{go} was not observed below 100 kPa; however, the value can be extrapolated from the exponential fit of the lower molar percentage data points and later confirmed by high-pressure measurements (Fig. 3 and Supplementary Figs. 37 and 44). This extrapolation is possible due to the exponential trend observed at a lower temperature (195 K), where all P_{go} values can be determined for high amino loading (Supplementary Figs. 28 and 29). Additionally, the nitro group exhibited a notable impact on the exponential decay of P_{go} as a function of n (Fig. 3d).

In situ gas sorption studies. The structures of **Zn-CAT**, **Zn-CAT-$(NH_2)_{100}$** and **Zn-CAT-$(NO_2)_{100}$** were also characterized by in situ powder X-ray diffraction under various acetylene pressures at 195 K (Supplementary Fig. 45) to further investigate the effect of bdc substitution and phase transformations.

Increasing the gas pressure resulted in a transition from a closed to open phase structure, which occurred at different pressures for the three samples. The gate-opening pressures, which correspond to the phase transition observed on the powder X-ray diffraction patterns, were observed at P_{go} = 0.04, 0.21 and 1.16 kPa for **Zn-CAT-$(NO_2)_{100}$**, **Zn-CAT** and **Zn-CAT-$(NH_2)_{100}$**, respectively. The difference in the parent structure can explain this difference. Below P_{go}, the powder X-ray diffraction patterns of activated MOFs (closed form) for **Zn-CAT-$(NH_2)_{100}$** and **Zn-CAT-$(NO_2)_{100}$** show a decrease and increase in the volume of the cell, respectively, compared to pristine **Zn-CAT**, as seen from the shift of the 100 peak. These results were confirmed by the crystal structure obtained from X-ray diffraction experiments (Supplementary Tables 1 and 2)[38]. The cell volume of activated **Zn-CAT-$(NO_2)_{100}$** (715.9 Å^3) is higher than that of **Zn-CAT** (703.6 Å^3) and **Zn-CAT-$(NH_2)_{100}$** (701.9 Å^3), which can be attributed to (1) the softer interaction of $-NO_2$ groups with the metal nodes and (2) the steric hindrance of the $-NO_2$ moiety, which further separates the aromatic part of the ligand. Therefore, the stabilization of the structure through π–π interactions is reduced, as observed for a pristine MOF[42].

For **Zn-CAT-$(NH_2)_{100}$**, the higher pressure needed for the gate opening to occur is explained by the initially more contracted structure owing to interactions between $-NH_2$ moieties and oxygen atoms from the metal paddle wheel[38]. Finally, all MOF structures are entirely open in the higher pressure range, and they display similar diffraction patterns (Supplementary Fig. 45d–f). Considering that the open and closed forms of each material are isostructural, the difference in the gate-opening pressure is attributed to the functionalized bdc–X linker.

Theoretical investigations of the gate-opening behaviour. To rationalize the effect of a linker on the thermodynamics of the gate-opening process, we applied theoretical thermodynamic models to the adsorption isotherms of **Zn-CAT** and its derivatives (Supplementary Information)[43,44]. Researchers have previously shown that a simple two-phase model provides a good description of gate opening in interpenetrated frameworks. The gate opening is an adsorption-driven first-order phase transition from a non-porous phase to a microporous phase. Here, the 'open phase' adsorption is described by a Langmuir-type fit of isotherms for all

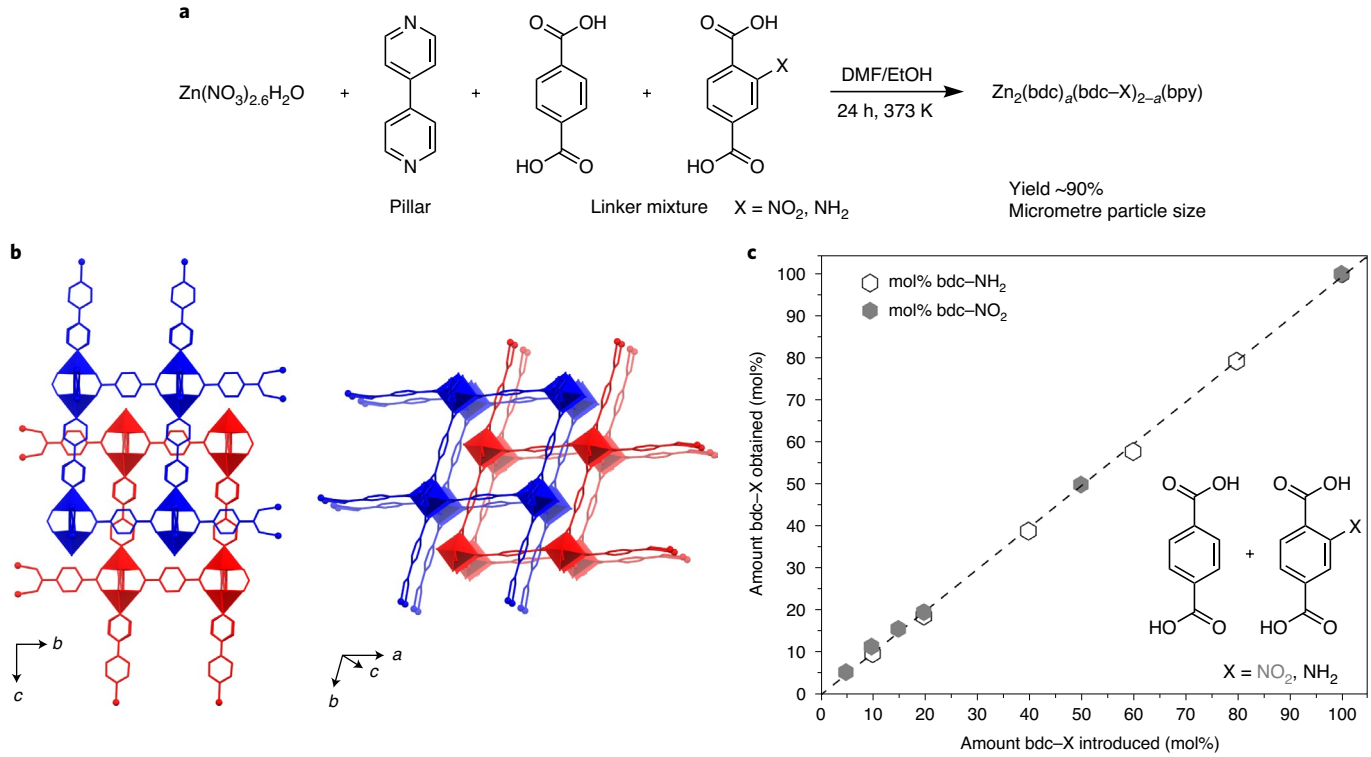

Fig. 2 | Presentation of the Zn-CAT-(X)*n* derivatives as soft porous crystal candidates. a, Synthetic scheme of **Zn-CAT-(X)*n*** materials, showing the different linkers: bipyridine, bdc and the functionalized bdc-X linkers (where X is $-NO_2$ or $-NH_2$). DMF, dimethylformamide. **b**, Left, crystal structure of activated **Zn-CAT** along the *b* axis; right, crystal structure of activated **Zn-CAT** along the *c* axis showing a pillar ligand connecting the two-dimensional layers. The twofold interpenetrated structures are shown in blue and red; the metal clusters (nodes) are shown as polyhedra, the linkers in stick representation. **c**, Molar percentage of the bdc-X linker within the material obtained as a function of the molar percentage of bdc-X introduced in the reaction. The obtained ratio was estimated from the ^{1}H NMR spectra of digested sample, and are available in Supplementary Figs. 2–14.

materials at 273 K. The free energy difference (ΔF) associated with the gate-opening process has been calculated based on the adsorption and desorption isotherms (Supplementary Information for the equations). This value indicates that **Zn-CAT** exhibits a relatively small free energy difference ($\Delta F = 5.2\,kJ\,mol^{-1}$) between the two phases (here, all energies are reported per unit cell). This value is slightly larger, but of a similar order of magnitude, than those of other gate-opening materials, such as $[Cu(4,4'\text{-bpy})(dhbc)_2]H_2O$ (dhbc = 2,5-dihydroxybenzoic acid), which has a ΔF of approximately $4\,kJ\,mol^{-1}$ (refs. [21,45]). The relatively small free energy difference between the two phases explains why the material readily opens upon adsorption of small guests.

However, the introduction of $-NO_2$ and $-NH_2$ substituents leads to a decrease in ΔF (Supplementary Table 3). The impact of $-NH_2$ was determined to be smaller than that of $-NO_2$. The more pronounced decrease in ΔF of **Zn-CAT-$(NO_2)_{100}$** is attributed to the repulsive interaction of the $-NO_2$ groups in the closed phase. Owing to the smaller energetic cost for gate opening, the opening is easier and occurs at lower gas pressures. This is particularly noticeable in the **Zn-CAT-$(NO_2)_{100}$** phase, where the free energy difference is almost zero, which implies that the material is truly bistable. Minute amounts of adsorbate trigger the gate-opening transition. This effect was more complex when $-NH_2$ groups were present. The introduction of $-NH_2$ groups in **Zn-CAT** decreased ΔF but did not lead to a decrease in the gate-opening (and closing) pressure. The effect is smaller than that of the $-NO_2$ groups because $-NH_2$ is a less bulky substituent. Therefore, the change in ΔF is not the dominant factor, and the driving force is the evolution of affinity in the open phase, discussed in detail later in the paper.

These results suggest the possibility of purposefully controlling the gate-opening and gate-closing pressures by introducing different ratios of functional groups. Additionally, the dependence of gate opening and closing on the molar ratio of amino or nitro functional groups is not unique to acetylene. Still, it is also applicable to CO_2, O_2 and CH_4, demonstrating the method's versatility (Supplementary Figs. 30–36).

Notably, the total adsorbed capacity does not considerably change for all **Zn-CAT-$(NH_2)_n$** compared to that of pristine **Zn-CAT** for acetylene gas at 273 K (Fig. 3c). The total adsorption capacity at higher loading in the **Zn-CAT-$(NH_2)_n$** series was recorded at a lower temperature ($T = 195$ K), demonstrating that the total capacity did not decrease for all **Zn-CAT-$(NH_2)_n$** series (Supplementary Figs. 28 and 29). Conversely, the capacity decreases up to 15% for **Zn-CAT-$(NO_2)_{100}$** (from 2.73 mol mol^{-1} to 2.32 mol mol^{-1}). This difference is expected due to the bulkier nitro moiety (van der Waals surface area of bdc–NO_2 = 249.2 Å^2) compared to the amino moiety (van der Waals surface area of bdc–NH_2 = 223.3 Å^2).

To better understand the origin of the counter-intuitive observation that the gate-opening pressure decreases after introducing a $-NO_2$ group into **Zn-CAT** but increases after introducing an $-NH_2$ group, quantum chemical calculations were carried out (Supplementary Information for computational details). For clarity, only C_2H_2 adsorption onto pristine **Zn-CAT** and fully substituted MOFs, that is, **Zn-CAT-$(NH_2)_{100}$** and **Zn-CAT-$(NO_2)_{100}$**, were considered. As shown in Supplementary Table 4, the binding energy (BE) of C_2H_2 with MOFs increased in the order **Zn-CAT-$(NH_2)_{100}$** (-9.3 kcal mol^{-1}) > **Zn-CAT** (-9.9 kcal mol^{-1}) > **Zn-CAT-$(NO_2)_{100}$** (-10.6 kcal mol^{-1}), where a more negative BE value indicates stronger

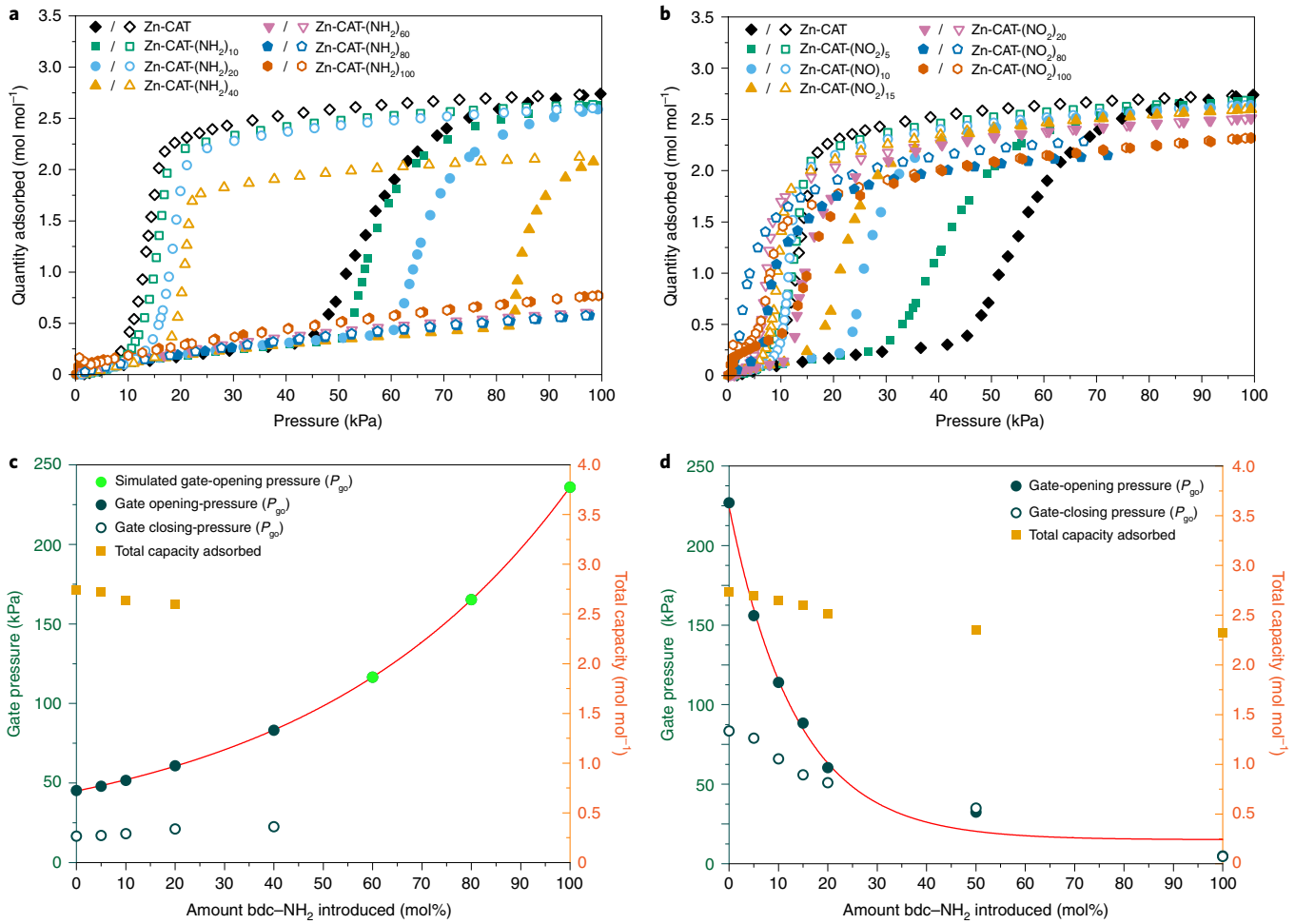

Fig. 3 | Tunable acetylene uptake and release sorptions. a, Acetylene (C_2H_2) adsorption isotherms for all **Zn-CAT-(NH$_2$)*n*** at 273 K. The **Zn-CAT** isotherm (black) was added for comparison. **b**, Acetylene (C_2H_2) adsorption isotherms for all **Zn-CAT-(NO$_2$)*n*** at 273 K. The **Zn-CAT** isotherm (black) was added for comparison. **c**, Acetylene (C_2H_2) gate-opening (green filled circle), predicted gate-opening (light green filled circles) and gate-closing (green empty circles) pressures for all **Zn-CAT-(NH$_2$)*n*** at 273 K. Total capacity (orange filled squares) as a function of molar percentage of $-NH_2$ in **Zn-CAT** if reached below 100 kPa. **d**, Acetylene (C_2H_2) gate-opening (green filled circles) and gate-closing (green empty circles) pressures for all **Zn-CAT-(NO$_2$)*n*** at 273 K. Total capacity (orange filled squares) as a function of molar percentage of $-NO_2$ in **Zn-CAT** if reached below 100 kPa. The total capacities were collected from the maximum uptake obtained in the adsorption isotherm. The gate-opening and gate-closing pressures were calculated from the adsorption and desorption isotherm inflexions at 273 K. The simulated gate-opening pressures were extrapolated from the exponential growth function with rate constant parameter.

C_2H_2 adsorption with increased energy stabilization. The results suggest that C_2H_2 adsorption begins to occur at a higher pressure for **Zn-CAT-(NH$_2$)$_{100}$** but at a lower pressure for **Zn-CAT-(NO$_2$)$_{100}$**, consistent with the experimental results.

The BE was decomposed into the interaction energy (E_{int}) between the MOF and C_2H_2 molecules and that of the adsorbed C_2H_2 molecules and the deformation energy (E_{def}) of the MOF structure by C_2H_2 adsorption. The E_{int} values were similar for C_2H_2 adsorption onto **Zn-CAT**, **Zn-CAT-(NH$_2$)$_{100}$** and **Zn-CAT-(NO$_2$)$_{100}$**, which is reasonable because the adsorption positions of C_2H_2 in these MOFs are similar (Supplementary Fig. 46). However, E_{def} differs considerably and is of the same order as that of P_{go}. The larger E_{def} for **Zn-CAT-(NH$_2$)$_{100}$** indicates that the introduction of the $-NH_2$ group into **Zn-CAT** results in a less flexible framework; thus, the gate-opening pressure increases. The less flexible framework occurs due to the hydrogen-bonding interactions of the $-NH_2$ group with the neighbouring bpy and carboxylate ligands (Supplementary Fig. 47a). The hydrogen-bonding interaction between the $-NH_2$ group and the bpy ligand weakened after C_2H_2 adsorption, confirmed by the increase in the NH_2–bpy distance (Supplementary Fig. 47a,b).

For **Zn-CAT-(NO$_2$)$_{100}$**, the introduced $-NO_2$ group results in a repulsive interaction with the carboxylate ligand (Supplementary Fig. 47c) in the guest-free structure. Consequently, the framework flexibility is increased to reduce the repulsive interaction, explaining the smaller E_{def} of **Zn-CAT-(NO$_2$)$_{100}$** than that of pristine **Zn-CAT**, hence decreasing the gate-opening pressure. Indeed, the $-NO_2$ groups do not exist in a repulsive position after C_2H_2 adsorption (Supplementary Fig. 47d). These results indicate that introducing substituents into parent MOFs can tune the flexibility of MOFs and readily change the E_{def} of the framework upon gas adsorption, making it possible to control the gate-opening gas adsorption, as observed from the experimental results.

Optimal conditions. Based on the insight into the structural dynamics of our system obtained from the combination of various characterization techniques and theoretical calculations, we used the amino group to efficiently adjust both P_{go} and P_{gc} for practical use at different temperatures (Fig. 4). Due to the limitation of actual physisorption instruments to 100 kPa pressure, we built a system capable of recording the acetylene physisorption at a higher

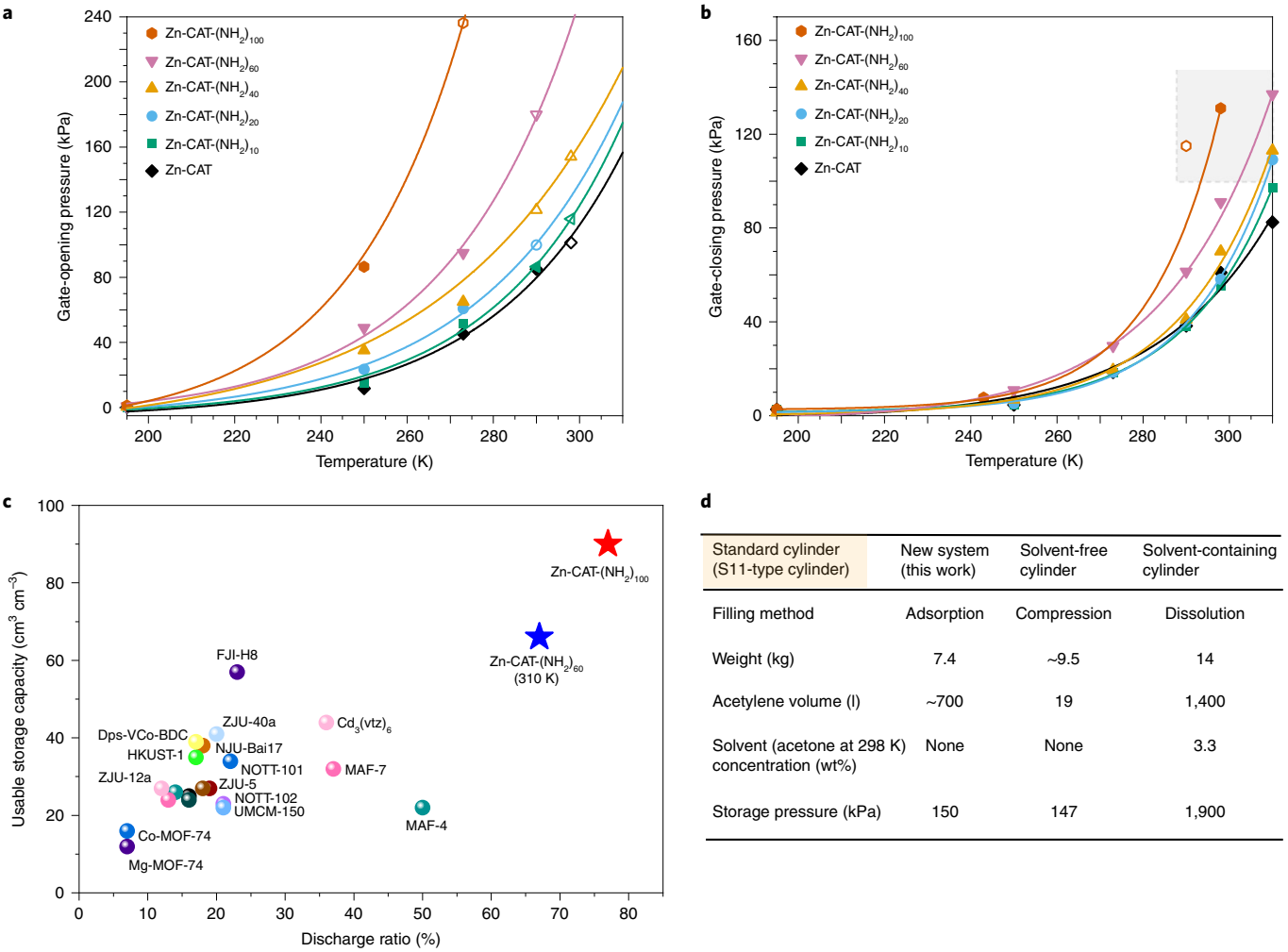

d

Standard cylinder (S11-type cylinder)	New system (this work)	Solvent-free cylinder	Solvent-containing cylinder
Filling method	Adsorption	Compression	Dissolution
Weight (kg)	7.4	~9.5	14
Acetylene volume (l)	~700	19	1,400
Solvent (acetone at 298 K) concentration (wt%)	None	None	3.3
Storage pressure (kPa)	150	147	1,900

Fig. 4 | Efficiency of Zn-CAT-(X)*n* for acetylene storage. a,**b**, Obtained (filled symbols) and predicted (empty symbols) gate-opening (**a**) and gate-closing (**b**) pressures of **Zn-CAT** and **Zn-CAT-(NH_2)*n*** as a function of temperature. The grey square shows the most suitable region for practical discharge pressure for acetylene gas release (100–150 kPa). **c**, Comparison of the usable storage capacities as a function of discharge ratio (the ratio of usable storage capacity at 100–150 kPa to uptake at 150 kPa) for acetylene storage of reported MOFs (MAF-4 (ref. [18]), MAF-7 (ref. [19]), $Cd_3(vtz)_6$ (ref. [20]), FJI-H8 (ref. [21]), NOTT-101 (ref. [22]), NOTT-102 (ref. [22]), UMCM-150 (ref. [22]), ZJU-40a (ref. [23]), ZJU-5 (ref. [24]), PCN-16 (ref. [22]), NJU-Bai17 (ref. [25]), HKUST-1 (ref. [22]), Dps-VCo-BDC (CPM-733-dps) (ref. [26]), UTSA-20 (ref. [22]), MOF-505 (ref. [22]), MFM-188 (ref. [27]), ZJNU-71 (ref. [28]), ZJU-12a (ref. [29]), Mg-MOF-74 (ref. [22]) and Co-MOF-74 (ref. [22])). **d**, Comparison of commercialized acetylene cylinders with an estimated **Zn-CAT-(NH_2)$_{100}$** filler system. The S11-type cylinder is a cylinder with 9.6 l inner volume.

pressure than 100 kPa, which has not been seen before, to the best of our knowledge (Supplementary Fig. 37). The optimal compressed condition must not exceed 200 kPa due to the acetylene's explosive behaviour above this pressure. The discharge gas should be above 100 kPa because the gas would not flow automatically below this pressure. Thus, it is possible, with this solid solution system, to fill at a low temperature to achieve a high adsorption amount at a low gate-opening pressure while releasing at room temperature above 100 kPa. The optimal conditions for the safe handling and use of compressed pure acetylene gas were tested for **Zn-CAT-(NH_2)$_{60}$** with a maximum released gas of 66 v/v at 100 kPa and 310 K (which is 67% of the cylinder content) and **Zn-CAT-(NH_2)$_{100}$**, which allowed the release of 77% of the cylinder content (~90 v/v) at 100 kPa and 298 K (Fig. 4 and Supplementary Fig. 44).

Our system has three main advantages compared to the state-of-the-art materials. First, when comparing the usable storage capacity of acetylene for **Zn-CAT-(NH_2)$_{100}$** with the reported MOFs, our material provides a usable storage capacity of ~90 v/v at 150 kPa and degassing at 100 kPa, both at 298 K, which is the highest among the reported MOFs (Fig. 4c and Supplementary Table 5). Second, **Zn-CAT-(NH_2)$_{100}$** achieves 77% of the amount released at 100 kPa, which is a crucial indicator of safety, as the unused or trapped acetylene is potentially dangerous (Fig. 4c). Compared to the MOFs reported for their high adsorption capacity, all retained at least 50% of acetylene in their pores. Third, the recyclability tests did not show any change in the uptake or release capacity, which contrasts with the conventional zeolite-type adsorbents that cannot be reused without strong heating reactivation (Supplementary Figs. 48 and 49).

For industrial development, we demonstrated that our flexible MOF adsorbents exhibit the following practical advantages for storing acetylene compared to the current solvent compression method (Fig. 4d): High acetylene purity is achieved as no solvents that can degrade or contaminate are present. The functionalized **Zn-CAT-(X)$_n$** can compress large quantities of acetylene (~117 v/v) at less than 200 kPa, allowing the development of smaller gas containers at low pressure with filling controlled via a pressure gauge and not by mass. Compared to the solvent-free

compression method, the adsorbed gas can be compressed in larger quantities in MOF pores (37-fold increase; Fig. 4d). Finally, the release pressure condition are easily manageable with the percent ratio of the amino group. Indeed, geographically different locations have different climates and thus different temperature regimes in which to operate the acetylene containers. Therefore, the tailor-designed nature of the **Zn-CAT-(X)$_n$** solid solution offers tunable uptake/release pressures at a desired temperature for various gases.

Conclusion

Herein, we demonstrated the design of a functional MOF with practical gate pressures via a modification of the molecular framework. The designed system has a mechanism by which the substituent exchange of the ligand controls the gate pressures of the target guest molecule by modulating the deformation energy of the interpenetrated framework. In the case of acetylene storage, these conditions were met using **Zn-CAT-(NH$_2$)$_{60}$** at 310 K and **Zn-CAT-(NH$_2$)$_{100}$** at 298 K, which allowed the release of more than 66% of acetylene at 100 kPa. This method is versatile, as it uses readily available MOFs and achieves the required performance with only minor modifications. We hope that these results will help the application of flexible MOFs to the practical storage of targeted gases using the discovery of cooperative adsorption phenomena.

Online content

Any methods, additional references, Nature Research reporting summaries, source data, extended data, supplementary information, acknowledgements, peer review information; details of author contributions and competing interests; and statements of data and code availability are available at https://doi.org/10.1038/s41557-022-00928-x.

Received: 28 May 2021; Accepted: 11 March 2022;
Published online: 21 April 2022

References

1. Matsuda, R. et al. Highly controlled acetylene accommodation in a metal–organic microporous material. *Nature* **436**, 238–241 (2005).
2. *Safetygram 13, Acetylene* (Air Products and Chemicals, 2014).
3. *Solvents for Acetylene Filling*. Doc. 225/19 (European Industrial Gases Association, AISBL, 2019).
4. Martin Bulow, S. B., Norman, D., Parkyns, D. & Sajik, W. M. Method and vessel for the storage of gas. WO1997016509, US patent (1999).
5. Kapelewski, M. T. et al. Record high hydrogen storage capacity in the metal–organic framework Ni$_2$(*m*-dobdc) at near-ambient temperatures. *Chem. Mater.* **30**, 8179–8189 (2018).
6. Li, B. et al. Porous metal-organic frameworks: promising materials for methane storage. *Chem* **1**, 557–580 (2016).
7. Moghadam, P. Z. et al. Computer-aided discovery of a metal–organic framework with superior oxygen uptake. *Nat. Commun.* **9**, 1378 (2018).
8. Vaidhyanathan, R. et al. Direct observation and quantification of CO_2 binding within an amine-functionalized nanoporous solid. *Science* **330**, 650–653 (2010).
9. Horike, S., Shimomura, S. & Kitagawa, S. Soft porous crystals. *Nat. Chem.* **1**, 695–704 (2009).
10. Warren, J. E. et al. Shape selectivity by guest-driven restructuring of a porous material. *Angew. Chem. Int. Ed.* **53**, 4592–4596 (2014).
11. Chang, Z., Yang, D.-H., Xu, J., Hu, T.-L. & Bu, X.-H. Flexible metal–organic frameworks: recent advances and potential applications. *Adv. Mater.* **27**, 5432–5441 (2015).
12. Schneemann, A. et al. Flexible metal–organic frameworks. *Chem. Soc. Rev.* **43**, 6062–6096 (2014).
13. Zhang, J.-P. & Chen, X.-M. Optimized acetylene/carbon dioxide sorption in a dynamic porous crystal. *J. Am. Chem. Soc.* **131**, 5516–5521 (2009).
14. Henke, S., Schneemann, A., Wütscher, A. & Fischer, R. A. Directing the breathing behavior of pillared-layered metal–organic frameworks via a systematic library of functionalized linkers bearing flexible substituents. *J. Am. Chem. Soc.* **134**, 9464–9474 (2012).
15. Jiang, H.-L., Makal, T. A. & Zhou, H.-C. Interpenetration control in metal–organic frameworks for functional applications. *Coord. Chem. Rev.* **257**, 2232–2249 (2013).
16. Martí-Gastaldo, C. et al. Side-chain control of porosity closure in single- and multiple-peptide-based porous materials by cooperative folding. *Nat. Chem.* **6**, 343–351 (2014).
17. Taylor, M. K. et al. Tuning the adsorption-induced phase change in the flexible metal–organic framework Co(bdp). *J. Am. Chem. Soc.* **138**, 15019–15026 (2016).
18. Horcajada, P. et al. How linker's modification controls swelling properties of highly flexible iron(III) dicarboxylates MIL-88. *J. Am. Chem. Soc.* **133**, 17839–17847 (2011).
19. Devic, T. et al. Functionalization in flexible porous solids: effects on the pore opening and the host–guest interactions. *J. Am. Chem. Soc.* **132**, 1127–1136 (2010).
20. Ramsahye, N. A. et al. Influence of the organic ligand functionalization on the breathing of the porous iron terephthalate metal organic framework type material upon hydrocarbon adsorption. *J. Phys. Chem. C* **115**, 18683–18695 (2011).
21. Kundu, T., Shah, B. B., Bolinois, L. & Zhao, D. Functionalization-induced breathing control in metal–organic frameworks for methane storage with high deliverable capacity. *Chem. Mater.* **31**, 2842–2847 (2019).
22. Mason, J. A. et al. Methane storage in flexible metal–organic frameworks with intrinsic thermal management. *Nature* **527**, 357–361 (2015).
23. Zhu, A.-X. et al. Tuning the gate-opening pressure in a switching pcu coordination network, X-pcu-5-Zn, by pillar-ligand substitution. *Angew. Chem. Int. Ed.* **58**, 18212–18217 (2019).
24. Horike, S., Inubushi, Y., Hori, T., Fukushima, T. & Kitagawa, S. A solid solution approach to 2D coordination polymers for CH_4/CO_2 and CH_4/C_2H_6 gas separation: equilibrium and kinetic studies. *Chem. Sci.* **3**, 116–120 (2012).
25. Fukushima, T. et al. Solid solutions of soft porous coordination polymers: fine-tuning of gas adsorption properties. *Angew. Chem. Int. Ed.* **49**, 4820–4824 (2010).
26. Zhang, J.-P., Zhu, A.-X., Lin, R.-B., Qi, X.-L. & Chen, X.-M. Pore surface tailored SOD-type metal-organic zeolites. *Adv. Mater.* **23**, 1268–1271 (2011).
27. Henke, S., Schmid, R., Grunwaldt, J.-D. & Fischer, R. A. Flexibility and sorption selectivity in rigid metal–organic frameworks: the impact of ether-functionalised linkers. *Chem. Eur. J.* **16**, 14296–14306 (2010).
28. He, Y., Krishna, R. & Chen, B. Metal–organic frameworks with potential for energy-efficient adsorptive separation of light hydrocarbons. *Energy Environ. Sci.* **5**, 9107–9120 (2012).
29. Duan, X., Cui, Y., Yang, Y. & Qian, G. A novel methoxy-decorated metal–organic framework exhibiting high acetylene and carbon dioxide storage capacities. *CrystEngComm* **19**, 1464–1469 (2017).
30. Pang, J. et al. A porous metal-organic framework with ultrahigh acetylene uptake capacity under ambient conditions. *Nat. Commun.* **6**, 7575 (2015).
31. Cai, J. et al. An amino-decorated NbO-type metal–organic framework for high C_2H_2 storage and selective CO_2 capture. *RSC Adv.* **5**, 77417–77422 (2015).
32. Wang, S.-Q. et al. High working capacity acetylene storage at ambient temperature enabled by a switching adsorbent layered material. *ACS Appl. Mater. Interfaces* https://doi.org/10.1021/acsami.1c06241 (2021).
33. Sun, X. et al. Tuning the gate opening pressure of a flexible doubly interpenetrated metal–organic framework through ligand functionalization. *Dalton Trans.* **47**, 13158–13163 (2018).
34. Schwedler, I. et al. Mixed-linker solid solutions of functionalized pillared-layer MOFs – adjusting structural flexibility, gas sorption, and thermal responsiveness. *Dalton Trans.* **45**, 4230–4241 (2016).
35. Foo, M. L., Matsuda, R. & Kitagawa, S. Functional hybrid porous coordination polymers. *Chem. Mater.* **26**, 310–322 (2014).
36. Lescouet, T., Kockrick, E., Bergeret, G., Pera-Titus, M. & Farrusseng, D. Engineering MIL-53(Al) flexibility by controlling amino tags. *Dalton Trans.* **40**, 11359–11361 (2011).
37. Chen, B. et al. A microporous metal–organic framework for gas-chromatographic separation of alkanes. *Angew. Chem. Int. Ed.* **45**, 1390–1393 (2006).
38. Gu, Y. et al. Structural-deformation-energy-modulation strategy in a soft porous coordination polymer with an interpenetrated framework. *Angew. Chem. Int. Ed.* **59**, 15517–15521 (2020).
39. Xiang, S., Zhou, W., Gallegos, J. M., Liu, Y. & Chen, B. Exceptionally high acetylene uptake in a microporous metal–organic framework with open metal sites. *J. Am. Chem. Soc.* **131**, 12415–12419 (2009).
40. Fukushima, T. et al. Modular design of domain assembly in porous coordination polymer crystals via reactivity-directed crystallization process. *J. Am. Chem. Soc.* **134**, 13341–13347 (2012).
41. Lescouet, T. et al. Homogeneity of flexible metal–organic frameworks containing mixed linkers. *J. Mater. Chem.* **22**, 10287–10293 (2012).
42. Ghoufi, A., Maurin, G. & Férey, G. Physics Behind the Guest-Assisted Structural Transitions of a Porous Metal–Organic Framework Material. *J. Phys. Chem. Lett.* **1**, 2810–2815 (2010).

43. Coudert, F.-X., Jeffroy, M., Fuchs, A. H., Boutin, A. & Mellot-Draznieks, C. Thermodynamics of guest-induced structural transitions in hybrid organic–inorganic frameworks. *J. Am. Chem. Soc.* **130**, 14294–14302 (2008).
44. Bousquet, D., Coudert, F. X. & Boutin, A. Free energy landscapes for the thermodynamic understanding of adsorption-induced deformations and structural transitions in porous materials. *J. Chem. Phys.* **137**, 044118 (2012).
45. Kitaura, R., Fujimoto, K., Noro, S.-I., Kondo, M. & Kitagawa, S. A. Pillared-layer coordination polymer network displaying hysteretic sorption: $[Cu_2(pzdc)_2(dpyg)]_n$ (pzdc = pyrazine-2,3-dicarboxylate; dpyg = 1,2-di (4-pyridyl)glycol). *Angew. Chem. Int. Ed.* **41**, 133–135 (2002).

Methods

Materials. All chemicals were used as received without any further purification. The 1,4-benzenedicarboxylic acid, 2-amino-1,4-benzenedicarboxylic acid, 2-nitro-1,4-benzenedicarboxylic acid and 4,4′-bipyridine were purchased from TCI. Zinc nitrate hexahydrate, ethanol (EtOH), DMF and other materials were purchased from Nacalai Tesque.

Synthesis of Zn-CAT and Zn-CAT-(X)$_n$ MOF series. The syntheses of **Zn-CAT** and the **Zn-CAT-(X)$_n$** series ($n = 0$ to 100% and X = –NH_2, –NO_2) were conducted following a method previously published, and they can be produced at 100 g scale[37]. Specifically, 1,4-benzenedicarboxylic acid is dissolved with the functionalized 1,4-benzenedicarboxylic acid (total 2 equiv., 20 mmol) in DMF (concentration [bdc linker] = 0.15 M) at 373.15 K for 15 min. An ambient solution of $Zn(NO_3)\cdot 6H_2O$ (2 equiv., 5.94 g, 20 mmol) in DMF (concentration [metal] = 0.4 M) was added to the stirring mixture at 373.15 K for 10 min. The 4,4′-bipyridine (1 equiv., 1.56 g, 10 mmol) was dissolved at room temperature in EtOH (concentration [pillar] = 0.1 M) and added to the reaction mixture. The mixture was kept at 373.15 K for 24 h. After cooling down to room temperature, the resulting precipitate was collected via centrifugation and washed three times with DMF (3 × 40 ml) and three times with EtOH (3 × 40 ml). The material was dried under vacuum at 323.15 K for 12 h to give a white/yellow powder in ~90 to 98% yields (6 to 6.9 g).

The ^{1}H NMR spectra. Each MOF was dissolved in 0.75 ml of DMSO-d_6 solvent and 10 µl of deuterated trifluoroacetic acid. The ^{1}H NMR spectra were recorded at 298.15 K at 400 MHz, where chemical shifts (δ in ppm) were determined with respect to tetramethylsilane (TMS) as an internal reference.

Thermogravimetric analysis. The thermal stability of all MOFs was measured under nitrogen flux with a heating rate of 5 K min^{-1} from 303.15 K to 773.15 K on a Perkin Elmer STA 6000 thermogravimetric analyser.

Powder X-ray diffraction. Powder X-ray diffraction measurements were performed on a Rigaku SmartLab X-ray diffractometer using Cu Kα radiation (wavelength $\lambda = 1.54178$ Å) in the two-theta range of 3–40° with a scanning rate of 5° min^{-1}.

Ultraviolet–visible absorption spectroscopy. UV spectra of all materials were measured on a JASCO V670 spectrophotometer from 700 to 200 nm. Samples were previously heated at 423 K under vacuum for 12 h before measurements.

Scanning electron microscopy analyses. Scanning electron microscopy images were collected with a HITACHI SU5000 microscope using a 3.0 kV acceleration voltage and 5 mm working distance. Samples were directly deposited on a conductive carbon tape.

Single-crystal X-ray diffraction. Measurements of single-crystal X-ray diffraction data for as-synthesized and activated **Zn-CAT-$(NO_2)_{100}$** were collected on beamline BL02B1 at the Japan Synchrotron Radiation Research Institute with 0.41270 Å radiation at 100 K and 195 K, respectively. Crystals were extracted from a mixture of DMF/EtOH into oil and mounted onto the goniometer for data collection. The structures were solved using SHELXT. Structure solution and refinement was performed within SHELXL on Olex2. Crystal information and details relating to the structural refinements are presented in Supplementary Tables 1 and 2. Crystallographic data for **Zn-CAT-$(NO_2)_{100}$** structures have been deposited in the Cambridge Crystallographic Data Centre (CCDC) with numbers 2036574 (as-synthesized structure) and 2036575 (activated structure).

Single gas adsorption isotherms. MOF samples were activated through thermal activation at 423 K for 12 h before measurement. The adsorption isotherms were measured with BELSORP-CRYO (C_2H_2 and CO_2) and BELSORP-MAX (C_2H_2, CO_2, CH_4 and O_2) volumetric adsorption equipment from Bel Japan. Targeted relative pressures in the range of 0.01–100 kPa were defined, and limits of excess and allowance amount were set to 5 and 10 cm^3 g^{-1}, respectively. Equilibrium conditions for each point were 0.03% pressure change within 300 s. The dead volume was determined using helium gas.

Gate-opening and gate-closing pressure and total capacity determination. The gate pressure points were determined at the inflection point of the adsorption and desorption isotherms. The total capacity values reported are the maximum amount of gas adsorbed by the material.

In situ powder X-ray diffraction coupled with gas sorption measurements. The measurements were performed on BELSORP-18PLUS (MicrotracBEL) automated volumetric sorption analysers, equipped with cryostat temperature controllers. The in situ powder X-ray diffraction/adsorption measurements were carried out using a Rigaku SmartLab with Cu Kα radiation connected to BELSORP-18PLUS volumetric adsorption equipment. Those apparatuses were synchronized with each other, and each powder X-ray diffraction pattern was obtained at each point of the sorption isotherms. The samples were first activated through external thermal activation at 423 K for 12 h and further 2 h internal activation at 423 K before measurement.

Acetylene high-pressure storage test set-up measurements. The experimental set-up used for acetylene storage measurements is shown in Supplementary Fig. 37. The gas manifold consisted of two lines fitted with a mass flow controller. One line was used to feed an inert gas (in our case, helium gas is used as the reference gas) before each experiment and as a gas purge after each acetylene measurement. The other line contained pure acetylene gas. In a typical experiment, 10 g of adsorbent powder was activated under vacuum at 423 K in a separate oven for 12 h. The vessel was filled with helium and plugged in the set-up. Before starting each experiment, the column was evacuated and heated at 423 K for 2 h before the acetylene filling at a flow rate of 50 cm^3 min^{-1}. The acetylene filling process was performed at low temperature (273 K or 243 K). After reaching the maximum loading, the vessel was slowly warmed to 290 K, 298 K or 310 K. The acetylene excess amount was released during the heating process. After filling, the desorption was made by vacuum pump until complete release of the gas occurred.

Data availability

X-ray crystallographic data have been deposited at the CCDC (http://www.ccdc.cam.ac.uk/) under CCDC no. 2036574 (as-synthesized **Zn-CAT-$(NO_2)_{100}$**) and no. 2036575 (activated **Zn-CAT-$(NO_2)_{100}$**). A copy of the data can be obtained free of charge via https://www.ccdc.cam.ac.uk/structures/. All other data supporting the findings of this study are available within the article and its Supplementary Information. Source data are provided with this paper. The source data for Supplementary Figs. 29–32 are available in Supplementary Data 3. Data are also available from the corresponding author upon reasonable request.

Acknowledgements

This work was supported by Air Liquide via the 2016 Air Liquide Scientific Challenge, a KAKENHI Grant-in-Aid for Specially Promoted Research (JP25000007), Scientific Research (S) (JP18H05262) and Early-Career Scientists (JP19K15584) from the Japan Society of the Promotion of Science. Synchrotron X-ray diffraction measurements were performed at the Japan Synchrotron Radiation Institute, Super Photon Ring – 8 GeV (proposal nos 2018B1820 and 2019A1136). We acknowledge iCeMS Analysis Centre for access to analytical facilities.

We are grateful to CNRS-Kyoto LIA 'SMOLAB'. In addition, we thank Air Liquide Japan, P. Ginet and L. Prost, as well as the technical staff for advice and experimental assistance.

Author contributions

S.K., C.L. and R.R. formulated the project. M.B. and C.L. synthesized the compounds and collected the gas adsorption data. M.B. and C.L. analysed all adsorption data. M.B. and C.L. collected and analysed the ^{1}H NMR, thermogravimetric analysis and powder X-ray diffraction data. K.-i.O. and K.S. collected and analysed the synchrotron X-ray diffraction data. A.L. and M.B. collected all scanning electron microscopy images and ultraviolet–visible spectroscopy and infrared analysis data. F.-X.C. performed the thermodynamics calculations. J.-J.Z. and S.S. performed the quantum chemical calculations. T.O. and C.L. built and collected the sorption data from the acetylene experimental set-up. M.B., K.-i.O., A.L., J.-J.Z., F.-X.C. and S.K. wrote the paper, and all authors contributed to revising the paper.

Competing interests

R. Réau is senior scientific director of research and development and group senior fellow of Air Liquide, France. C. Lavenn, research project manager, and T. Ogawa are employed at Air Liquide Laboratories Innovation Campus in Tokyo, Japan. S. Kitagawa was partially funded by Air Liquide in the frame of a collaboration research agreement between Air Liquide and Kyoto University. The other authors do not declare any competing interests.

Additional information

Supplementary information The online version contains supplementary material available at https://doi.org/10.1038/s41557-022-00928-x.

Correspondence and requests for materials should be addressed to Susumu Kitagawa.

Peer review information *Nature Chemistry* thanks the anonymous reviewers for their contribution to the peer review of this work.

Reprints and permissions information is available at www.nature.com/reprints.